Updating dynamic noise models with moving magnetoencephalographic (MEG) systems

J. D. López[1]*, Member, IEEE, T. M. Tierney[2], A. Sucerquia[3], F. Valencia[4], Member, IEEE, N. Holmes[5], S. Mellor[2], G. Roberts[5], R. Hill [5], R. Bowtell[5], M. Brookes[5], G. Barnes[2]

[1]Engineering Faculty, Universidad de Antioquia UDEA, Calle 70 No 52-21, Medellín, Colombia
[2]Wellcome Centre for Human Neuroimaging, UCL Institute of Neurology, London, UK, WC1N 3BG
[3]Engineering Faculty, Instituto Tecnológico Metropolitano ITM, Cra 65, 98A-75, Medellín, Colombia
[4]Energy Center, Faculty of Mathematical and Physical Sciences, University of Chile, 8370451 Santiago, Chile
[5]Sir Peter Mansfield Imaging Centre, School of Physics and Astronomy, University of Nottingham, University Park, Nottingham, UK, NG7 2RD

Corresponding author: José David López (e-mail: josedavid@udea.edu.co).

ABSTRACT Optically pumped magnetometers have opened many possibilities for the study of human brain function using wearable moveable technology. In order to fully exploit this capability, a stable low-field environment at the sensors is required. One way to achieve this is to predict (and compensate for) changes in the ambient magnetic field as the subject moves through the room. The ultimate aim is to account for dynamically changing noise environments by updating a model based on measurements from a moving sensor array. We begin by demonstrating how an appropriate environmental spatial noise model can be developed through Free-energy based model selection. We then develop a Kalman-filter based strategy to account for dynamically changing interference. We demonstrate how such a method could not only provide realistic estimates of interfering signals when the sensors are moving, but also provide powerful predictive performance (at a fixed point within the room) when both sensors and sources of interference are in motion.

INDEX TERMS Magnetoencephalography, Kalman Filter, Magnetic Sensors, Noise Cancellation, Magnetic Noise, Magnetometers, Magnetic Field Measurement, Optically Pumped Magnetometers.

I. INTRODUCTION

Magnetoencephalography (MEG) is a non-invasive brain imaging method based on the measurement of femto-Tesla magnetic field change outside of the head [1]. The technique can provide spatially resolved and direct estimates of neuronal current flow which update millisecond by millisecond [2]. Until recently, MEG systems have been large static devices which occupy the centre of a shielded room. Now, optically pumped magnetometers (OPM) have demonstrated the measurement of fields from the human brain [3]. As these sensors are small and light, they can be worn in a helmet and are no longer bound to remain at a fixed location within the room [4], stimulating a great deal of neuroscientific and clinical interest. This new technology also introduces an additional challenge to MEG; not only must the brain's electrical activity be estimated, but the highly non-stationary changes in environmental interference due to sensor movement must also be accounted for. In this, paper we set out a possible theoretical framework to address this issue.

Principally, this work is motivated by a practical necessity. Currently, the most sensitive and compact commercial OPM systems [5] are based on SERF (spin exchange relaxation free) devices, which provide measures of magnetic field but are optimally sensitive at zero field. This means the field at the sensor head must be nulled in some way. This can be achieved internally (using on-board coils) and therefore typically (to date) with the subject nominally static [3], [6]; or externally by augmenting the static shielding factor of the room with bi-planar coils surrounding the subject [4], [7]. For example, within a typical three-layer MEG shielded room one will expect a residual static field of 20 nT with a 5 nT/m gradients [7] whilst the dynamic range of a typical SERF device is ±1.5 nT (at maximum resolution). At present, however, the use of additional coils constrains the region of movement of the subject (around ±15 cm) and attenuates, but does not remove, any sensor interference due to head-movement. The aim of this paper is to provide a comprehensive and continuously updated model of the environmental noise generated outside and inside the room. Given accurate

knowledge of head-position and trajectory in this way not only could the impact of movement through static fields be mitigated, but also the changing structure of the higher frequency interference be predicted. We foresee these methods will require a mixture of both external and internal coil compensation strategies, but ultimately both will require a model of the environmental noise.

Here we borrow concepts from the classical empirical Bayesian framework for M/EEG brain imaging [8], [9] and apply them to modelling magnetic fields external to the sensor array. The main distinction is that for the first time we have a moving MEG sensor which can provide us with novel samples from the environment; as the sensor is moving and the environment is changing, we also must track these changes. The use of dynamic estimators in M/EEG is not new and extends from Kalman filters [10], [11] to complex non-stationary off-line model estimators [12], [13]. In this work we make use of the Kalman filter, a Markovian optimal quadratic estimator [14] widely used for tracking and estimating states and disturbances (see [15], [16] for reviews on the field). It has been used on several fields for de-noising, tracking (e.g. sources of epileptic foci [11], [17], characterising disturbances and, more commonly, for estimating process states on modern control systems [18]–[20].

This paper proceeds as follows. We begin by explaining how the Bayesian M/EEG brain imaging framework can be extended to estimate environmental noise. We demonstrate our approach by showing how candidate models of the external noise space can be compared in the stationary case. We introduce the Kalman filter as a practical way of exploiting the information gained from moving sensors. Given an optimal source space model we make use of a Kalman filter to update and track non-stationary dynamics. Finally, we demonstrate how this framework extends to the case of a single moving sensor tracking moving sources of disturbance.

II. METHDOS

A. ROOM SPACE INVERSE PROBLEM

Traditional M/EEG brain imaging consists of finding the sources of neural activity within the brain, typically modelled by a cortical manifold of current dipoles. Here the set of sensors is located within the search space, and the objective is to populate the surrounding space with magnetic dipoles that will generate the magnetic fields measured by the sensors (See

Figure 1 Fig. 1). This will allow us to both characterise sources of disturbance and estimate the magnetic field at every usable location of the shielded room by computing a new forward problem.
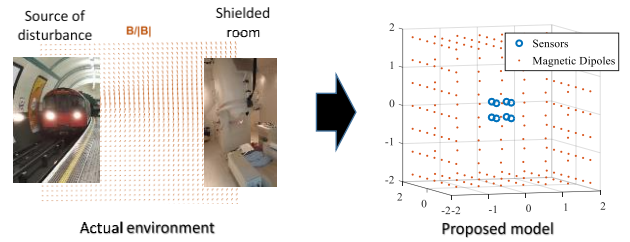

Figure 1. Proposed spatial model. Environmental magnetic noise can be approximate by a shell of magnetic dipoles surrounding the measurement space. Here we assume that the shell is cubic but that each point of the shell contains a magnetic dipolar source at arbitrary orientation. The first objective is to select an optimal scale for this shell based on environmental noise data measured at the sensors (blue circles).

Let us define the environmental magnetic fields recorded by N_c (theoretical) tri-axial sensor locations as $B \in \Re^{3N_c \times N_t}$, for N_t time samples. Then, N_d magnetic dipoles are placed around the region of the room that will be mapped (on a cubic shell in this case), these dipoles have fixed locations and unknown orientation. The magnetic moments of these dipoles are the unknowns: $m \in \Re^{3N_d \times N_t}$. The propagation model between dipoles and sensors can be modelled with an extended version of the general linear model:

$$B = Lm + HJ + e \qquad (1)$$

Where $L, H \in \Re^{3N_c \times 3N_d}$ are gain (lead-field) matrices linking magnetic field B to external sources m (magnetic dipoles) and brain (cortical) current flow $J \in \Re^{3N_d \times N_t}$ respectively (and with different units) , and e represents unexplained additive noise. For clarity (as here we focus on estimation of m) we can parcel the component of B due to brain activity (HJ, which will be small compared to the environmental interference) into a composite error term ϵ:

$$B = Lm + \epsilon \qquad (2)$$

The propagation model used to compute the lead-field matrix L corresponds to the magnetic dipole equation:

$$L = \frac{\mu_0}{4\pi} \left(\frac{3r\left(\vec{l_m} \cdot (\vec{r} - \vec{r}_d)\right) - r^2 \vec{l_m}}{r^5} \right) \qquad (3)$$

that relates the moment orientation $\vec{l_m}$ of a magnetic dipole at $\vec{r}_d$ with a sensor location $\vec{r}$. The reconstruction of the expected amplitudes $\hat{m}$ is performed with the traditional Maximum Likelihood optimisation [21]:

$$\hat{m} = QL^T(LQL^T + Q_\epsilon)^{-1}B, \qquad (4)$$

with $Q \in \Re^{3N_d \times 3N_d}$ being the prior source (i.e. environmental interference) space covariance matrix. As in the traditional solutions for brain imaging, Q should include prior information such as spatial smoothness (LORETA [22]), data driven projections (Beamformers –EBB [23], [24], or sparsity (Multiple Sparse Priors –MSP [8]), etc. For our tests here, we use EBB as it presented the better performance on preliminary tests (specially in computational burden). In EBB an empirical

prior source covariance matrix Q_{EBB} is estimated based on the measured data B and the lead-field matrix L [24]:

$$Q_{\text{EBB}} = h_1 \text{diag}(\Gamma);$$
$$\Gamma_{\text{i}} = \left. 1 \middle/ {}_{\delta_i} \right. (L_i^T(BB^T)^{-1}L_i)^{-1}, \tag{5}$$

$\forall i = 1, \dots, 3N_d$, where L_i is the i-th row of L, and $\text{diag}(\cdot)$ is an operator that converts a vector into a diagonal matrix. Each dipole projection is normalised with $\delta_i = (L_i^T L_i)^{-1}$. With respect to the noise variance prior $Q_\epsilon \in \Re^{3N_c \times 3N_c}$, for simplicity we define it as an identity matrix $Q_\epsilon = h_0 I$, with h_0 being a regularisation parameter [25].

The parameters $\{h_0, h_1\}$ can be optimised by an expectation-maximization algorithm, using the negative variational free energy F as a cost function [26]. With this approach, every solution of the OPM room-level inverse problem will be related to a final F value that can be used for model comparison. The Free energy is a trade-off between accuracy and complexity of the model. Summarizing, the accuracy depends on both the relation between the data covariance and the model-based covariance, penalised by the size (determinant) of the model-based covariance. The complexity, on the other hand, penalises the difference between the prior at parameter level and the optimised posterior values (see [27] for practical examples of using Free energy for model comparison, and [28] for implementation details within this framework).

B. STATE SPACE REPRESENTATION

The traditional general linear model of (2) is static. Here we must deal with non-stationary noise sources and moving sensors. Therefore, we have extended this model to the well-known discrete-time state-space representation (See [29] for a wider explanation on dynamical models):

$$x_k = A_k x_{k-1} + R_k u_k + w_{k-1} \tag{6}$$
$$y_k = C_k x_k + D_k u_k + \epsilon_k \tag{7}$$

The essence of this representation is that the current value of the states x_k in (6) can be estimated from their weighted previous estimate $A_k x_{k-1}$ (i.e., Markovian) and a projected input $R_k u_k$, plus some unknown state disturbances w. The output of the system y_k in (7) depends on both states and inputs, plus some output (sensor) noise ϵ.

Applied to our problem, the states will be the magnitude of the magnetic fields at the dipoles m and the output will be the magnetic fields measured by the sensors B; therefore, the output matrix C becomes the lead-field matrix L. For this specific scenario, there is no direct input (autonomous system), then $u = 0$ and the state-space representation becomes:

$$m_k = A_k m_{k-1} + w_{k-1} \tag{8}$$
$$B_k = L m_k + \epsilon \tag{9}$$

Contrary to M/EEG, where we have prior knowledge to construct the state transition matrix $A_k \in \Re^{3N_d \times 3N_d}$ (see [10],

[11]), here we lack a temporal model of the sources of disturbance; thus, we make a simple data-driven selection by setting: $A_k = \text{diag}(\Gamma_k)$, with Γ_k being computed as in (5) with only data recorded at sample time k. With this selection, we give updating priority to those regions more likely to be active at sample time k due to the current data B_k projected over the states and normalised. There are many other possible variations for this transition matrix which we touch on in the discussion.

Note that the state-space representation allows one to decompose the uncertainty into sensor noise $\epsilon \in \Re^{3N_c \times N_t}$ and other sources of disturbance $w \in \Re^{3N_d \times N_t}$. In future, prior knowledge of these disturbances could be introduced in w_k (the trains follow the same path, the air conditioner always has the same power spectrum, etc.).

C. KALMAN FILTER IMPLEMENTATION

To our knowledge, the simplest candidate to deal with our specific problem is the Kalman filter, a Markov model estimator of the discrete-time state-space system representation [14]. The Kalman filter is a dynamic extension of the Maximum Likelihood optimisation of (4), which here is known as the Kalman gain:

$$G_k = P_k^- L^T (L P_k^- L^T + Q_\epsilon)^{-1} \tag{10}$$

The main difference with the traditional static scenario of (4) is that the source space covariance matrix P_k is dynamically updated at the Kalman filter.

The Kalman filter begins with a prediction stage, where both current expected values of the states m_k and their variance P_k are predicted based on their previous sample estimation:

$$m_k^- = A_k m_{k-1}: \qquad \text{1. Prediction in states}$$
$$P_k^- = A_k P_{k-1} A_k^T + W: \qquad \text{2. Prediction in posterior covariance of states}$$

Where the super index $(\cdot)^-$ implies prediction (i.e., only based on temporal modelling), and W is the state disturbance covariance $E(ww^T) = W$.

The next step is to compute the Kalman gain with (10), which is followed by a correction stage using the current value of the measurements B_k:

$$G_k = P_k^- L^T (L P_k^- L^T + Q_\epsilon)^{-1}: \qquad \text{3. Compute Kalman gain}$$
$$m_k = m_{k-1} + G_k (B_k - L m_k^-): \qquad \text{4. Update on states}$$
$$P_k = (I_{N_d} - G_k L) P_k^-: \qquad \text{5. Update on posterior covariance of states}$$

Note that for a perfect scenario, $G_k L = I_{N_d}$ and the uncertainty on the states would be zero; i.e., the state covariance matrix P_k is the term to be minimised through time at the Kalman filter.

For this room-level inverse problem, the Kalman filter parameters can be initialised as follows:

- Sensor noise covariance Q_ϵ: The regularisation parameter h_0 from $Q_\epsilon = h_0 I_{3N_d}$ can be computed with any regularisation strategy [30]. Here we assume same noise levels over the whole simulation; therefore, we just compute a general cross validation with prior data [31].
- Initial state moments m_0: They can be initialised by solving the EBB inverse problem for the first sample time.
- State disturbance covariance W and posterior state covariance P_0: In absence of prior information, we can initialise both with identity matrices: $P_0 = W = I_{3N_d}$.

D. EXPERIMENTAL SET-UP

We propose the following simulation workflow to show the proof of principle for our approach:

1. We demonstrate how it is possible to use model selection in order to compare between different environmental source spaces.
2. We test the Kalman filter and show that it can improve on stationary estimates when the sources of interference are non-stationary.
3. We extend this formalism to a moving sensor array.
4. Then, we show how the Kalman filter formulation can be used to update a moving source of noise model whilst the sensors themselves are moving.

The end goal is for a wearable system that can be used to estimate and update a model of the sources of magnetic noise in the environment. This model would be updated as the subject moves around the room and as the environmental noise conditions change. Given such a model, we can make a prediction of the sensor level field changes required to maintain the system at its optimal operating point and minimize the influence of environmental noise.

III. RESULTS

A. FINDING AN OPTIMAL SHELL TO DESCRIBE THE EXTERNAL NOISE

For this work we will assume an optimal shell, at some scale, on which we can place sources that will well describe the environmental noise. In this first scenario, we show how we can use Free energy for model comparison among possible shells. Importantly, the Free energy value comes with no knowledge of the ground truth.

This test consists of placing $N_c = 8$ tri-axial sensors (i.e., 24 individual single-axis sensors) equally distributed in a *usable* space of $40 \times 40 \times 40$ cm, and $N_d = 218$ magnetic dipoles on a cubic shell surrounding them. The magnetic dipoles shell has 15 possible distances to the centre of the room: $d = \{0.5, 0.6, \dots, 1.9\}$ m. We simulated two magnetic dipoles with uncorrelated waveforms (one sinusoid with random frequency between 1 and 10 Hz and one chirp

sweeping the same frequency range). Both simulated sources sit on one of the shells and are placed randomly with free orientation. We test with 100 trials of 1 s at 100 Hz sample frequency. The solver used is EBB over three different signal-to-noise levels: SNR = $\{-10, 0, 10\}$ dB. We used Free energy as the objective function to estimate the true shell containing the sources. We plot Free energy relative to the maximum observed over all models, with the best (most likely) model at zero Free energy.

Fig. 2 shows corrected Free energy results after 100 trials per layer computed with EBB within SPM12[1]. Each figure panel shows a different shell containing the sources: $d = \{0.6, 1.1, 1.8\}$ m (near, mid, and far from the centre of the shielded room) for the three tested SNRs. Note that the peak Free energy metric always coincides with the true shell, and that the larger the true shell the less important its position (as the fields have become more homogenous at a distance).
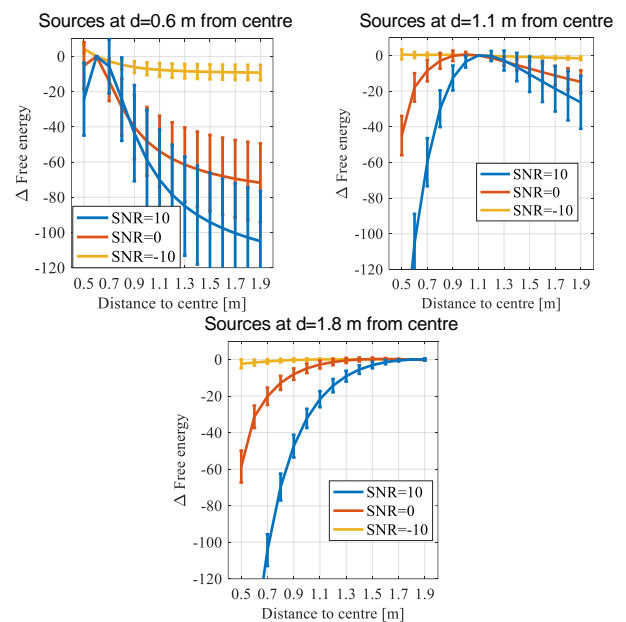

Figure 2. Modelling the impact due to different shells of magnetic dipoles. Here there are three simulated cubic shells with nearest faces situated at 0.6, 1.1 and 1.8m from the room centre. In each simulation, a shell contains two magnetic interfering sources at 10 (blue), 0 (orange) or -10 (yellow) dB SNR. Based on the sensors within a 40 cm cube at the centre of the room, we can compare shell models as these shells increase in size (x-axis). The three curves (blue, orange, yellow) show the model evidence for 15 different candidate shells.

The main purpose of this simulation is to demonstrate that it is possible to use model comparison (with no knowledge of ground truth) to decide upon an optimal shell containing environmental noise sources. In practice, we would expect this stage, which assumes stationarity, to be based on data extending over a long period of time. This would then give an appropriate spatial support to models which account for dynamic changes in source activity.

---

[1] https://www.fil.ion.ucl.ac.uk/spm/

B. TESTING THE KALMAN FILTER

Now that an appropriate spatial basis to model the interfering sources has been constructed, we introduce and motivate the use of the Kalman filter. The aim here is to account for dynamically changing noise environments using measurements from moving sensor arrays. The Kalman filter is Markovian, it has access to the previous system state, and for this reason we compare it to two extremes. The first, in which the system is assumed to be stationary (as in the majority of M/EEG brain imaging) using the traditional full-window EBB implemented on SPM12 (SPM-EBB) [24], [28]. The second in which the same EBB algorithm only has access to the current sample (Sample-EBB). Note that Sample-EBB is a worst-case scenario, used here to provide us with a minimal performance measure, which has no knowledge of anything but the present sample. Note that, For the full SPM-EBB algorithm, we removed the temporal projector [32] –a singular value decomposition of sensor level data which provides a useful pre-whitening and de-noising function -for a fair comparison with the other solvers.

For this experiment we keep the same number of sensors, sources and SNR as outlined above and assume that the shell model is established (the grid of dipoles is fixed at $d = 1.2$ m). Now that we have enough space inside the shell, we have also augmented the size of the *usable* space to 1 m^3 and placed the 8 tri-axial sensors at the corners of this space (larger space allows wider subject movement).

Here we address the problem of non-stationary temporal dynamics; for example, an air-conditioning system turning on and off. To construct a realistic dynamic environment, we simulate three sinusoidal sources for 5 s periods, one at the beginning, one at the middle, and one at the end of the window. The location of the sources (on the shell) and their frequency randomly varied across 100 trials of 10 s each.

The three algorithms were used to create estimates of the true source distribution. Note that the use of Free energy for model comparison now becomes problematic as each solver uses different time windows and therefore different data. As a metric of fit that would also penalize over fitting, we positioned a virtual sensor at the centre of the room and compared the data at this sensor due to the estimated model with the data due to the true model. As this virtual sensor was not used in the fit it provides a measure of the generalizability of the model. Fig. 3 shows this set-up with the three sources (black), the set of sensors (blue), and the waveform at the virtual sensor (brown).

Fig. 4A shows the variance explained at the measurement sensors under the different models. As the SNR decreases, the models, predictably, can account for less of the measured data. The best models however will not necessarily be those that explain the most sensor data, as these models may not generalize across new measurement locations. In order to remove this over-fitting concern, we looked at a virtual sensor within the centre of the room- which was not used to fit the

model. Fig. 4B shows the how well the estimated model predicted the data measured at this sensor.
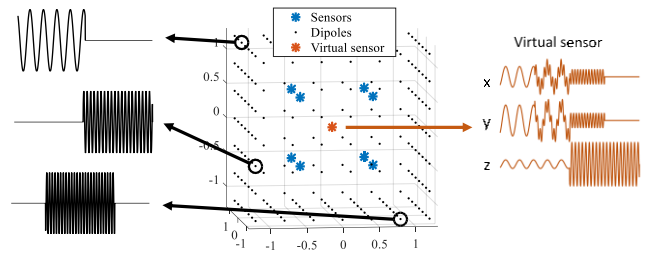

Figure 3. Example of a single trial realization of the configuration used. Three magnetic dipoles with different, non-stationary, time-series (left of figure) are placed randomly at the walls of the shell. Eight tri-axial sensors (blue asterisks) are used to measure these fields. A source estimate based on these measurements is made and this is estimate is projected back to a tri-axial virtual sensor (brown asterisk) at the centre of the room.

A. Variance explained at real sensors

B. VE at virtual sensor

C. Spatial correlation at source level
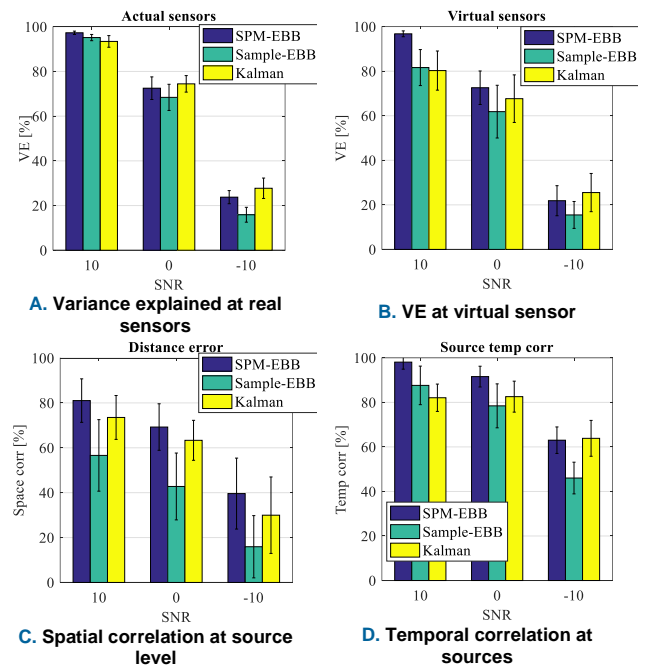
D. Temporal correlation at sources

Figure 4. Tests with dynamic sources (average of 100 trials). (A) The sensor level variance explained by the different algorithms. (B) The data explained at the virtual sensor, although like A, cannot be due to over-fitting. (C) The correlation between the true source distribution (over space) and the estimated source distribution and (D) The temporal correlation between the true and estimates sources at the true source locations.

We also computed the spatial (Fig. 4C) and temporal Fig. 4D) correlation at source level. Spatially, we computed the correlation between the power estimated across the source distribution and the power within true source distribution (only three random active dipoles per trial). The temporal correlation was computed by comparing the true and estimated time-series at the known source locations. Note that for all these metrics, the Kalman filter and SPM-EBB methods have similar performance and improve upon model estimates using Sample-EBB.

It should be noted that had we included a de-noising stage (e.g. a temporal projector) within the SPM-EBB algorithm,

this algorithm would have outperformed the Kalman filter (as the de-noised principle signal components could have been extracted from the full time-series, removing a great deal of noise). However, the main aim of this example was to create a baseline for the next experiment, where we begin to move the tri-axial sensor, precluding the use of a continuous stationary data segment.

C. MOVING SENSOR, WITH FIXED NON-STATIONARY NOISE

Ultimately, we wish to exploit the mobility of the sensor array to sample fields over a greater volume and hence further elaborate the model of environmental noise. Here we repeat the previous test (with 3 sources of non-stationary noise at different locations in each trial) but only with a single tri-axial sensor that we move through the *usable* space. Fig. 5 shows an example of the trajectory used here (Fig. 5, coloured line). We modulated the sensor location across the three axes with sinusoids at frequencies between 1 and 5 Hz. This meant that within a 10s window (the sensor crosses five times at each point, i.e. 2s period) the sensor traversed the whole of the usable space. We quantified SNR (which depends on sensor position) as the average SNR over the complete sensor trajectory. Note that this strategy requires an update of the forward model at each sample time ($L_k \in \Re^{3 \times 3N_d}$) precluding the use of the stationary SPM-EBB solver.
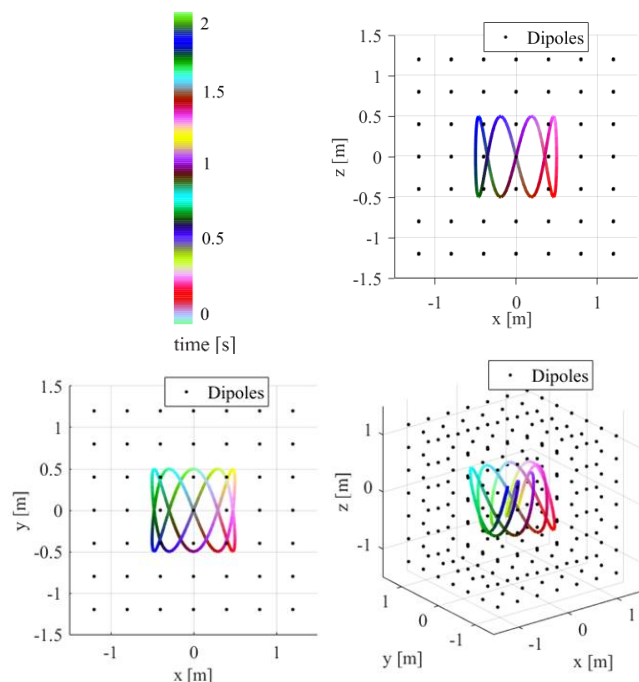

Figure 5. A single moving tri-axial sensor used to estimate the interference model. Here the 3 sources of non-stationary interference were again (as in Fig. 3) randomly positioned on the shell for each trial. The sensor was modulated sinusoidally across the usable space of 1 m³. The colours indicate the sensor position over time. The goal once again was to use this moving sensor data to build a model to predict magnetic field changes at a virtual sensor in the centre of the room.

Based on this moving sensor data, the Kalman filter was able to effectively track the magnetic field dynamics with over 70 % of accuracy for SNR = 0 dB. Fig. 6A shows the average variance explained (VE) by the prediction at the virtual sensor over 100 trials with the three SNR levels. Fig. 6B shows the single-trial comparison between the true and predicted virtual sensor signals (SNR = 0 dB) for Sample-EBB (top) and Kalman (lower panel) approaches. The main difference of note is that the Kalman filter estimate evolves smoothly whereas the sample-EBB produces impulsive estimates of the time-series. Note that the waveform being predicted is non-stationary and that the measurement sensors are in constant motion relative to the virtual sensor.
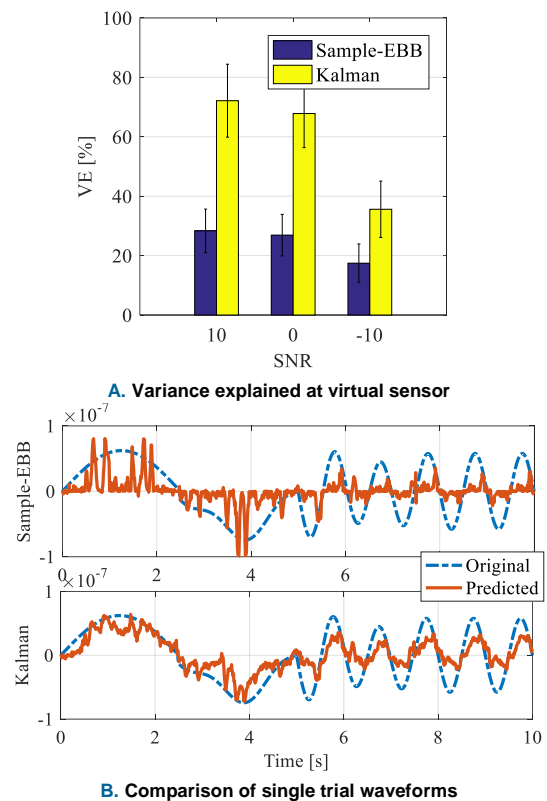

A. Variance explained at virtual sensor

B. Comparison of single trial waveforms

Figure 6. Prediction of signal at static virtual sensor based on measurements from a single tri-axial sensor moving within a shell containing 3 non-stationary noise sources (A) Average variance explained by the Sample-EBB (blue) and Kalman (yellow) models over 100 trials. (B) Single trial waveform comparison at the virtual sensor. Top panel shows sample-EBB in which the estimates are impulsive (the algorithm has no access to the past). Lower panel shows the smoothly evolving Kalman filter estimate.

D. MOVING SENSOR WITH MOVING STATIONARY NOISE SOURCE

In our final scenario, we extend the benchmark to deal with a moving source –such as a train crossing under the room, or another person moving within the room- whilst the sensor array is also moving. Here, we use a single sinusoidal source which moves around the room following the path shown in Fig. 7 (coloured). The tri-axial sensor was set up to follow the 3D sinusoidal-shape trajectory of Fig. 5. Fig. 7 shows the (moving) sensor measurements (red traces –note the

significant distortion) due to the moving source (colour coded according to location). The right panel shows the true signal at the virtual tri-axial sensor fixed at the centre of the room. We test the performance of both solvers (Sample-EBB and Kalman) with Variance Explained at the virtual sensor and the distance (tracking) error between the true and estimated source location. The distance metric is the Euclidean distance between the peak source estimate and the true source location; note however that the peak source estimate is quantized by the source spacing of 23 cm).
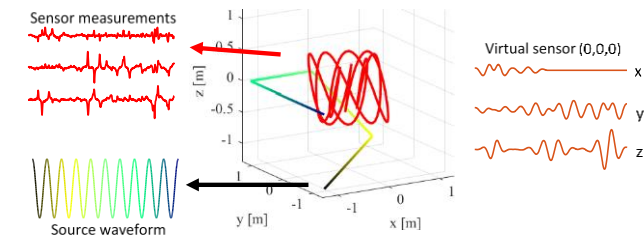

Figure 7. Moving sensors (red) with moving interference source (multi-coloured). The trajectories of the tri-axial sensor (red) and the source (graded from black to blue) are shown in the middle panel. The corresponding time-series in the left panel. Note how the sinusoidal time series due to the moving source looks highly distorted at the virtual sensor (right panel, brown) and almost unrecognisable based on the sensor measurements (left panel, red).

Fig. 8A shows the sample by sample tracking error for Sample-EBB (top) and Kalman (lower panel) with SNR = 10 dB for a single trial of data. Note how the Kalman filter, after an initialisation period (~1s), begins to track the movement of the source (ideal performance, given the grid quantization, is shown by red traces). The sample EBB-SPM algorithm, by contrast, is unable to track the source location. On average (Fig. 8B), the Kalman filter distance error is comparable to the grid spacing.
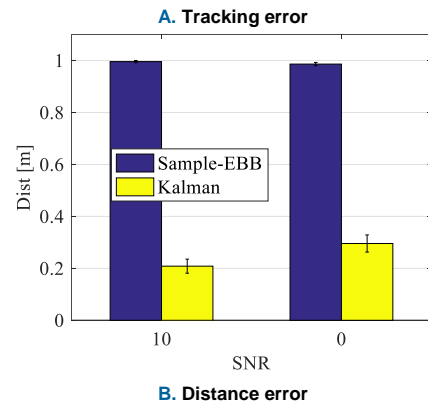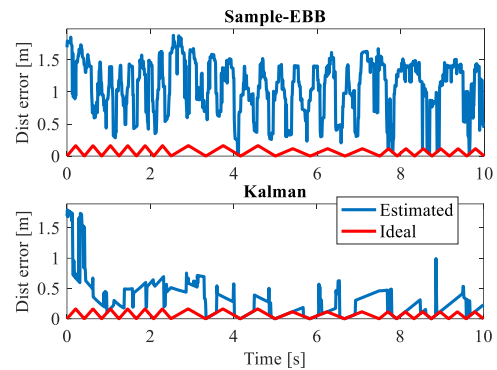

Figure 8. Moving tri-axial sensor updating a model of a moving source (A) Tracking distance error for one trial for the Sample-EBB (top) and the Kalman filter (lower panel). The ideal error (red) is non-zero as the source spaced is quantized with a grid-spacing of 23 cm. Note the tracking convergence of the Kalman filter after 1sec. (B) The average distance between the estimated and true source location for sample EBB (blue) and Kalman (yellow). Note the Kalman error is comparable to the grid spacing.

Fig. 9A shows the average variance explained at the static virtual sensor for two noise levels SNR = $\{10, 0\}$ dB after 100 simulations. As expected, the Kalman filter outperformed the sample EBB and, despite the challenging recording scenario, was able to predict more than 70 % of the variance. Fig. 9B shows a comparison of the predicted waveforms (single trial) at the static virtual sensor with the ground truth (blue) at a SNR = 0 dB. Again, note that the sample EBB can provide good impulsive estimates at the signal extrema (top panel), yet the Kalman filter provides smoothly evolving estimates over time. This result is encouraging considering the complexity of the problem faced and the absence of any filtering or information about the source trajectory.
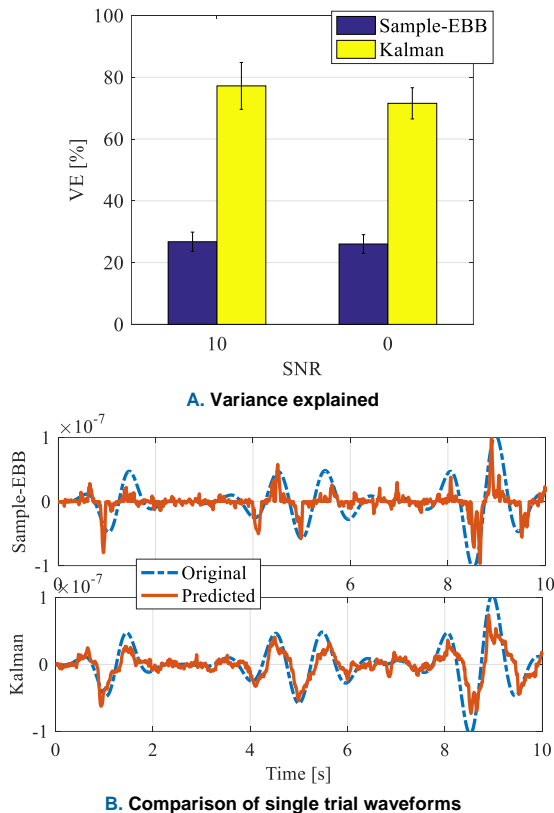
A. Variance explained

B. Comparison of single trial waveforms

Figure 9. Model predictions at static virtual sensor for a moving tri-axial sensor and moving interference source (A) Variance explained by the Sample-EBB (blue) and Kalman filter (yellow) models. (B) Single trial time-series estimates (orange) at the static virtual sensor as compared to ideal performance (blue dotted) for sample-EBB (top panel) and Kalman filter (lower panel).

IV. DISCUSSION

Magnetoencephalography is entering a new era of wearable arrays in order to measure brain function during natural human behaviour. A pre-requisite to measure brain function is to be able to account for the dynamically changing noise environment. Here we demonstrate how mobile OPM arrays could be used to build up dynamic models of environmental noise, and how these models can be updated as the sensors move around the room.

Here we used classical M/EEG brain imaging methods to estimate and update environmental noise models. The approach is attractive as these models are familiar to the community, and in contrast to models of brain function, models of external interference should be much more straightforward and tractable.

The first step in the modelling of environmental noise is to create some spatial support on which magnetic sources lie. This comparable to defining a cortical manifold in which we allow current to flow. Unlike the cortical manifold, based on subject anatomy, the true environmental manifold will be a complex structure, which factors in the Earth's field, nearby traffic and elevator shafts, amongst other things. Here we assume that these external fields can be approximated by a cubic shell containing evenly spaced but randomly oriented

magnetic dipoles. We demonstrate how the dimensions of this cube can be optimized using model evidence to arrive at the most accurate description of the interference with the least complexity. The optimal shape, dimension and grid spacing of this support will vary from site to site but can be optimized in exactly the same way as has been done for the cortex using model evidence [33]–[35].

Given a spatial model to accommodate possible interfering sources, the next problem is to track them in time. We demonstrated its feasibility by performing a simple, single source reconstruction and comparing it with a traditional estimator (SPM-EBB) and a sample by sample version of the same algorithm (Sample-EBB, which becomes the baseline). We then tested these solvers with a dynamic environment where sources were switched on and off (like elevators, air conditioners and underground trains). Importantly, once the sensors begin to move, traditional approaches – which assume a constant spatial relationship between source and signal over time- are no longer applicable. However, we have shown that the Kalman filter is able to accommodate these non-stationary changes by virtue of its Markovian update scheme.

Perhaps the most challenging scenario was the tracking of a moving source (the elevator, the train, someone else in the room) with a single tri-axial sensor that was also in motion. The complexity of the problem is evident on Fig. 4. However, the Kalman filter managed to track the source trajectory and reconstruct up to 70 % of the field at a static virtual sensor.

It is worth noting that these results were achieved without using many current alternatives for model prediction commonly used in control systems and navigation [18]. For example, trains, elevators, air conditioning systems would have specific features: they would follow the same trajectory, have the same frequency spectrum, etc. In future developments, this prior knowledge could be fed into the term w in (8). Another possible direction for innovation is in the choice of the transition matrix A_k. Here we used a transition matrix based on the most recent beamformer source space estimate (the most likely next active sources will be the current active sources). However, another alternative would be to consider ARMA models generated from long recordings within the room [36].

At present, the empirical phase of this work is constrained by the dynamic range of the OPM sensors (approx. ±1.5nT with maximum ADC resolution) as compared to the noise field in the room with gradients of ~5nT/ metre [4], [7]. The next empirical stages will be a combination of external coils to reduce the remnant fields [7] and the use of less sensitive devices (but with greater dynamic range) to characterize the very large fields within the shielded room. Once this first stage is complete and an approximate environmental noise model (where the errors between predicted and measured field do not exceed the dynamic range of the OPMs) can be constructed then we hope to be able to dynamically adjust the OPM null point (with internal coils) dependent on position. This should ultimately allow us not only to create ever maturing and more

precise models of the environmental noise; but should also allow a greater repertoire and range of subject movement.

REFERENCES

[1] M. S. Hämäläinen and R. J. Ilmoniemi, "Interpreting measured magnetic fields of the brain: estimates of current distributions," 1984.

[2] S. Baillet, "Magnetoencephalography for brain electrophysiology and imaging," *Nat. Neurosci.*, vol. 20, no. 3, 2017.

[3] E. Boto *et al.*, "A new generation of magnetoencephalography: Room temperature measurements using optically-pumped magnetometers," *Neuroimage*, vol. 149, pp. 404–414, Apr. 2017.

[4] E. Boto *et al.*, "Moving magnetoencephalography towards real-world applications with a wearable system," *Nature*, vol. 555, no. 7698, pp. 657–661, Mar. 2018.

[5] V. K. Shah and R. T. Wakai, "A compact, high performance atomic magnetometer for biomedical applications," *Phys. Med. Biol.*, 2013.

[6] S. Knappe, T. Sander, and L. Trahms, "Optically-Pumped Magnetometers for MEG," in *Magnetoencephalography*, Berlin, Heidelberg: Springer Berlin Heidelberg, 2014, pp. 993–999.

[7] N. Holmes *et al.*, "A bi-planar coil system for nulling background magnetic fields in scalp mounted magnetoencephalography," *Neuroimage*, vol. 181, pp. 760–774, Nov. 2018.

[8] K. Friston *et al.*, "Multiple sparse priors for the M/EEG inverse problem," *Neuroimage*, vol. 39, no. 3, pp. 1104–1120, Feb. 2008.

[9] D. Wipf and S. Nagarajan, "A unified Bayesian framework for MEG/EEG source imaging," *Neuroimage*, vol. 44, pp. 947–966, 2009.

[10] A. Galka, O. Yamashita, T. Ozaki, R. Biscay, P. Valdes Sosa, and P. Valdés-Sosa, "A solution to the dynamical inverse problem of EEG generation using spatiotemporal Kalman filtering," *Neuroimage*, vol. 23, no. 2, pp. 435–453, Oct. 2004.

[11] E. Giraldo-Suarez, J. D. Martinez-Vargas, and G. Castellanos-Dominguez, "Reconstruction of Neural Activity from EEG Data Using Dynamic Spatiotemporal Constraints," *Int. J. Neural Syst.*, 2016.

[12] M. Woolrich, P. Chiarelli, D. Gallichan, J. Perthen, and T. Liu, "Bayesian inference of hemodynamic changes in functional arterial spin labelling data," *Magn. Reson. Med.*, vol. 56(4), pp. 891–906, 2006.

[13] S. Castaño-Candamil, J. Höhne, J. D. Martínez-Vargas, X. W. An, G. Castellanos-Domínguez, and S. Haufe, "Solving the EEG inverse problem based on space-time-frequency structured sparsity constraints," *Neuroimage*, 2015.

[14] R. E. Kalman, "A New Approach to Linear Filtering and Prediction Problems," *Trans. ASME, J. Basic Eng.*, vol. 82, pp. 35–45, 1960.

[15] S. I. Aanonsen, G. Nævdal, D. S. Oliver, A. C. Reynolds, and B. Vallès, "The Ensemble Kalman Filter in Reservoir Engineering--a Review," *SPE J.*, 2009.

[16] J. D. Hamilton, *Time series analysis*. New Jersey: Princeton University Press, 1994.

[17] A. Yan *et al.*, "Automatic seizure detection using Stockwell transform and boosting algorithm for long-term EEG," *Epilepsy Behav.*, 2015.

[18] F. Auger, M. Hilairet, J. M. Guerrero, E. Monmasson, T. Orlowska-Kowalska, and S. Katsura, "Industrial applications of the kalman filter: A review," *IEEE Trans. Ind. Electron.*, 2013.

[19] R. G. Brown and P. Y. C. Hwang, *Introduction to Random Signals and Applied Kalman Filtering with Matlab Exercises*. Wiley, 2012.

[20] L. Ljung, "Asymptotic behavior of the extended Kalman filter as a parameter estimator for linear systems," *IEEE Trans. Automat. Contr.*, vol. 24, no. 1, pp. 36–50, Feb. 1979.

[21] A. M. Dale and M. Sereno, "Improved Localization of Cortical Activity By Combining EEG and MEG with MRI Cortical Surface Reconstruction: A linear approach.," *J. Cogn. Neurosci.*, vol. 5, pp. 162–176, 1993.

[22] R. D. Pascual-Marqui, C. M. Michel, and D. Lehmann, "Low Resolution Electromagnetic Tomography: A new method for localizing electrical activity in the brain," *Int. J. Psychophysiol.*, vol. 18, pp. 49–65, 1994.

[23] K. Sekihara, S. S. Nagarajan, D. Poeppel, A. Marantz, and Y. Miyashita, "Application of an MEG eigenspace beamformer to reconstructing spatio-temporal activities of neural sources," *Hum. Brain Mapp.*, vol. 15, no. 4, pp. 199–215, Apr. 2002.

[24] P. Belardinelli, E. Ortiz, G. Barnes, U. Noppeney, and H. Preissl, "Source Reconstruction Accuracy of MEG and EEG Bayesian Inversion Approaches," *PLoS One*, vol. 7, no. 12, p. e51985, Dec. 2012.

[25] J. Sarvas, "Basic mathematical and electromagnetic concepts of the biomagnetic inverse problem," *Phys. Med. Biol.*, vol. 32, no. 1, pp. 11–22, 1987.

[26] K. Friston, J. Mattout, N. Trujillo-Barreto, J. Ashburner, and W. Penny, "Variational free energy and the Laplace approximation," *Neuroimage*, vol. 34, pp. 220–234, 2007.

[27] W. D. Penny, "Comparing Dynamic Causal Models using AIC, BIC and Free Energy," *Neuroimage*, vol. 59, no. 1, pp. 319–330, 2012.

[28] J. D. López, V. Litvak, J. J. Espinosa, K. Friston, and G. R. Barnes, "Algorithmic procedures for Bayesian MEG/EEG source reconstruction in SPM," *Neuroimage*, vol. 84, pp. 476–487, Jan. 2014.

[29] L. Ljung and T. Glad, *Modeling of Dynamic Systems*, First. Prentice Hall, 1994.

[30] R. Grech *et al.*, "Review on solving the inverse problem in EEG source analysis," *J. Neuro Eng. Rehabil.*, vol. 5, no. 1, p. 25, 2008.

[31] G. H. Golub, M. Heath, and G. Wahba, "Generalized Cross-Validation as a Method for Choosing a Good Ridge Parameter," *Technometrics*, vol. 21, no. 2, p. 215, May 1979.

[32] C. Phillips, M. D. Rugg, and K. J. Friston, "Anatomically Informed Basis Functions for {EEG} Source Localization: Combining Functional and Anatomical Constraints," *Neuroimage*, vol. 16, pp. 678–695, 2002.

[33] R. N. Henson, J. Mattout, C. Phillips, and K. J. Friston, "Selecting forward models for MEG source-reconstruction using model-evidence," *Neuroimage*, vol. 46, pp. 168–176, 2009.

[34] J. D. López, W. D. Penny, J. J. Espinosa, and G. R. Barnes, "A general Bayesian treatment for MEG source reconstruction incorporating lead field uncertainty," *Neuroimage*, vol. 60, no. 2, pp. 1194–1204, 2012.

[35] L. Troebinger, J. D. Lopez, A. Lutti, S. Bestmann, and G. Barnes, "Discrimination of cortical laminae using MEG," *Neuroimage*, vol. 102, no. P2, pp. 885–893, 2014.

[36] L. Ljung, "System Identification," in *Signal Analysis and Prediction*, Springer, 1998, pp. 163–173.